



Cite this: DOI: 10.1039/c9nr09816j

## Using FRET to measure the time it takes for a cell to destroy a virus†

Candace E. Benjamin,<sup>‡</sup> Zhuo Chen,<sup>‡</sup> Olivia R. Brohlin,<sup>‡</sup> Hamilton Lee,<sup>‡</sup> Arezoo Shahrivarkevishahi,<sup>‡</sup> Stefanie Boyd,<sup>‡</sup> Duane D. Winkler<sup>‡</sup> and Jeremiah J. Gassensmith<sup>‡</sup>\*<sup>a,c</sup>

The emergence of viral nanotechnology over the preceding two decades has created a number of intellectually captivating possible translational applications; however, the *in vitro* fate of the viral nanoparticles in cells remains an open question. Herein, we investigate the stability and lifetime of virus-like particle (VLP) Q $\beta$ —a representative and popular VLP for several applications—following cellular uptake. By exploiting the available functional handles on the viral surface, we have orthogonally installed the known FRET pair, FITC and Rhodamine B, to gain insight of the particle's behavior *in vitro*. Based on these data, we believe VLPs undergo aggregation in addition to the anticipated proteolysis within a few hours of cellular uptake.

Received 18th November 2019,  
Accepted 31st March 2020

DOI: 10.1039/c9nr09816j

rsc.li/nanoscale

### Introduction

Virus-like particles (VLPs)—proteinaceous nanoparticles engineered from viruses—have emerged as an accepted technology in clinical therapeutics.<sup>1,2</sup> These macromolecular structures closely resemble their original parent virus but are non-infectious, as they lack their original genetic material and cannot self-replicate. They retain, however, their capacity for efficient multimeric self-assembly when propagated in heterologous systems such as yeast or bacteria<sup>3</sup> and their quaternary structure is held together by strong but non-covalent interactions. In recent years, chemical bioconjugation of the coat proteins with synthetic ligands to induce new properties has emerged as a growing field of “chemical virology”.<sup>4</sup> These hybrid synthetically modified bio-based nanoparticles have gained considerable momentum as a scaffold for the precise installation of small molecules, additional functional proteins, and even inorganic nanoparticles. These characteristics define VLPs as an excellent platform for the development of highly specialized imaging, drug delivery, and sensing technologies.<sup>5–8</sup> Generally, without the installation of specific localization or escape moi-

eties on the VLP, it is well known that that these particles typically localize in endosomal compartments<sup>9</sup> and are destined for lysosomal degradation. This has influenced rational design such that the decreased pH associated with the lysosome has been used to control drug release with pH sensitive polymers,<sup>10</sup> changes in electrostatic binding<sup>11</sup> and to even measure the pH of the compartment.<sup>12</sup> Largely absent in the literature has been a mechanistic effort to understand what happens to the supramolecular structure of the virus once taken in by the cell. This information potentially can open new avenues of design centered around stimuli responsive behavior—in particular, we seek an understanding of the apparent time a VLP has to live as a supramolecular structure following uptake.

To investigate the intactness of the VLP, we chose to employ Förster resonance energy transfer (FRET), a well-known non-radiative distance dependent energy transfer between a pair of donor and acceptor molecules.<sup>13</sup> This phenomenon has been utilized in the design of biological probes,<sup>14</sup> chemical sensors,<sup>15</sup> and light harvesting devices<sup>16</sup> but is most recognized for its use in studying inter- and intramolecular protein interactions. FRET has been successfully employed to elucidate protein folding,<sup>17,18</sup> misfolding,<sup>19</sup> aggregation,<sup>20</sup> and dissemination<sup>21–23</sup> as its key attribute is that it is a “photonic ruler” that emits light based on the proximity of compatible fluorophores. The attached donor and acceptor fluorophores must fulfill two requirements: firstly, sufficiently overlapping emission and excitation spectra must exist such that the emission of the donor fluorophore can excite the group state of the acceptor. Secondly, the two moieties must be within a few nanometers of each other for this transfer of energy to occur efficiently. This technology is amenable for the study of a

<sup>a</sup>Department of Chemistry and Biochemistry, University of Texas at Dallas, Richardson, Texas 75080, USA. E-mail: gassensmith@utdallas.edu

<sup>b</sup>Department of Biological Sciences, University of Texas at Dallas, Richardson, Texas 75080, USA

<sup>c</sup>Department of Bioengineering, University of Texas at Dallas, Richardson, Texas 75080, USA

†Electronic supplementary information (ESI) available. See DOI: 10.1039/c9nr09816j

‡First two authors are equal contributors.

variety of substrates<sup>24,25</sup> and we have harnessed it here to aid in qualitatively evaluating VLP degradation following endocytosis in model immune and cancer cell lines to draw conclusions on particle lifetimes.

There are a variety of VLPs currently in use that run the gamut of size, shape, and host origin, which makes it exceedingly difficult to make general statements on these particles; therefore, we choose to focus solely on Q $\beta$ . This porous icosahedral particle is 28 nm in diameter and its shape and structure allow for the loading of small molecules in its interior *via* diffusion<sup>26</sup> or direct conjugation to interiorly directed amino acids.<sup>27</sup> The VLP has been widely used as a drug delivery

agent,<sup>28–31</sup> cancer immunotherapeutic,<sup>32,33</sup> and has shown promise in clinical trials for adjuvant free vaccination<sup>34–36</sup> attributable to the functional handles and its repetitive surface structure. The surface of Q $\beta$  contains two cysteine residues at positions 74 and 80 that daisy-chain each of the 180 14.1 kDa subunits together providing most the structural integrity of the particle. The resulting disulfide bonds are easily functionalized through dibromomaleimide chemistry without affecting the stability of the VLP<sup>37</sup> and is an orthogonal reaction to a second functionalization of the coat protein located at lysine residues 2, 13, 16 and the N-terminus, which are necessary for our proposed system (Fig. 1A and Scheme 1).

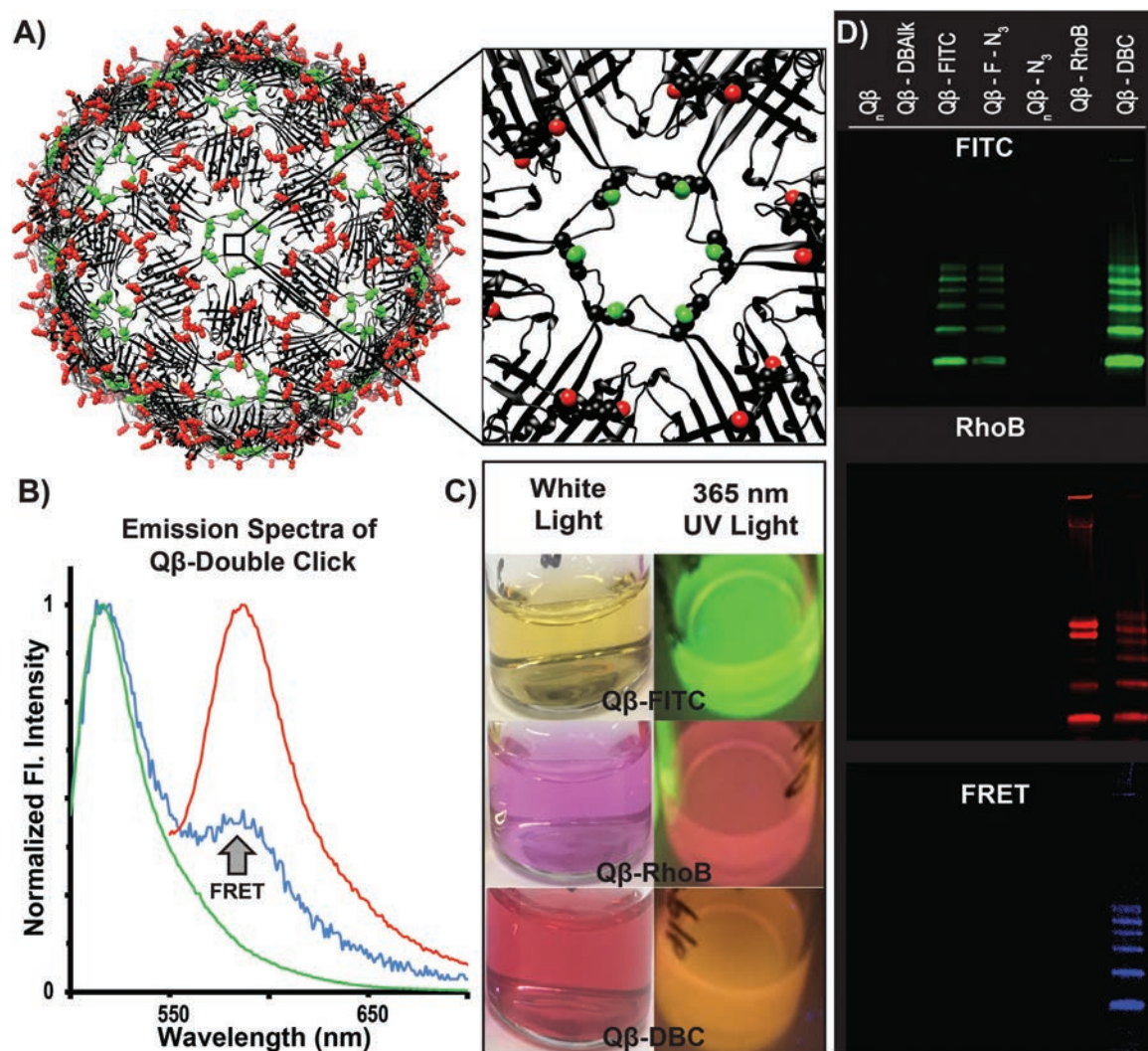
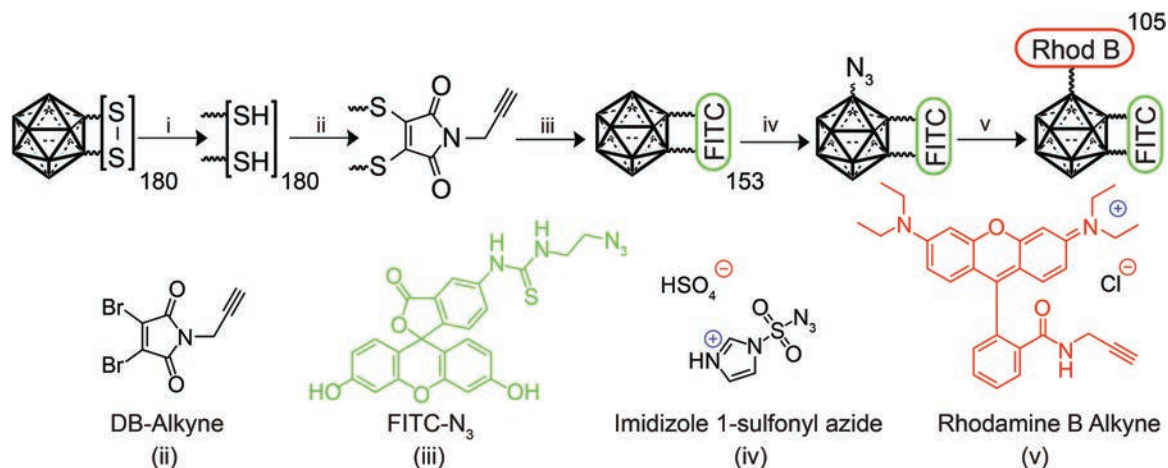


**Fig. 1** (A) Chimera rendering of the Q $\beta$  capsid with the cysteine and free amine residues labeled in green and red respectively. The inset shows the hexameric pore with the heteroatoms highlighted in green (sulfur) and red (nitrogen). (B) Fluorescence emission spectra of the attached fluorophore. The green line indicates FITC ( $\lambda_{\text{ex}}$ : 490 nm/ $\lambda_{\text{em}}$ : 520 nm), the red line shows rhodamine emission ( $\lambda_{\text{ex}}$ : 520 nm/ $\lambda_{\text{em}}$ : 590 nm), and the blue line shows the existence of FRET between the two fluorophores. (C) Images of the product at subsequent stages of conjugation. (D) Non-reducing SDS-PAGE gel images of Q $\beta$  conjugates after each step of conjugation. Green fluorescence can be seen only in lanes where Q $\beta$  has been conjugated to FITC which is the same for the red fluorescence image and rhodamine attachment. The red fluorescence seen in the Q $\beta$ -RhoB well results from a small amount of aggregated protein – the addition of a large number of positively charged fluorophores leads to capsid instability without dibromomaleimide conjugation. In lane 7, when the construct is excited at 490 nm and the emission obtained at 590 nm, only Q $\beta$  with both fluorophores shows a signal.



**Scheme 1** Schematic representation of the two copper catalyzed click reactions and relevant bioconjugation reactions performed to achieve the final conjugate. All steps are detailed in the Experimental section. Q $\beta$  is reduced (i), to yield free thiols which are then conjugated to an alkyne functionalized dibromomaleimide (ii). FITC is added *via* CuAAC (iii), the capsid is then subject to a diazo transfer reaction (iv) and another CuAAC reaction is used to attach Rhodamine B (v) to create the final product.

In this work, we install the FRET pair fluorescein isothiocyanate (FITC) and Rhodamine B (RhoB) to investigate the intactness of the Q $\beta$  VLP following cellular uptake. The ordered amino acid sequence present on the capsid surface allow for site specific dye installation thus we propose a four-part orthogonal synthetic procedure to attach the aforementioned fluorophores *via* copper catalyzed azide–alkyne cyclization (CuAAC) “click” chemistry to yield a FRET active VLP with efficient energy transfer capabilities. We measured the distance between neighboring thiol and amine groups we intend to functionalize using a Chimera generated structure (1QBE) and found that these handles are well within the reported<sup>38,39</sup> Förster distance of  $\sim 45$  Å – ranging from 18 to 38 Å in distance (Fig. S1†). The ordered installation of the FITC-RhoB FRET pair on the VLP surface coupled with the close proximity of the fluorophores results in a 46.74% energy transfer efficiency. Given the proteinaceous nature of the VLP, our initial hypothesis was that proteases will destroy the secondary structure, causing the collapse of the quaternary structure, which will separate the fluorophores within the endosome/lysosomal compartment and therefore cause a decrease in the FRET efficiency and signal.

## Materials and methods

### Synthetic procedures

**Expression and purification of Q $\beta$  VLPs ( $n$ Q $\beta$ ).** The expression and purification of Q $\beta$  VLPs was done by using a published procedure,<sup>27</sup> which is reproduced here in brief. The plasmids were gifts from Prof. M. G. Finn of the Georgia Institute of Technology. A 10 mL of starter culture of *E. coli* BL21DE3 cells with the plasmid were amplified to 500 mL of SOB media (100  $\mu$ g mL<sup>-1</sup> kanamycin) at 37 °C until the OD<sub>600</sub> was 0.9–1.0. To that, 1 mM (final concentration) of isopropyl

$\beta$ -D-1-thiogalactopyranoside (IPTG) was added to induce the expression at 37 °C overnight. Cells were harvested by centrifuging using a Fiberlite F10 rotor at 10 500 rpm (19 510g) for 1 h at 4 °C, followed by re-suspending into 70 mL of 0.1 M potassium phosphate buffer (pH 7.00). Cells were lysed in a cell homogenizer and the lysate was centrifuged in a Fiberlite F10 rotor at 10 500 rpm (19 510g) for 1 h at 4 °C. The pellet was discarded, and ammonium sulfate was added into the supernatant to produce a final concentration of 2 M and allowed to incubate with rotation for at least 1 h at 4 °C. The suspension was centrifuged using a Fiberlite F10 rotor at 10 500 rpm (19 510g) for 1 h at 4 °C. The pellet was re-suspended in 10 mL of 0.1 M potassium phosphate buffer (pH 7), and an equal volume solution of *n*-butanol and chloroform (1 : 1) was added. The solution was vortexed and pelleted by centrifuge in a Fiberlite F10 rotor at 10 500 rpm (19 510g) for 30 min at 4 °C. The top aqueous layer was carefully recovered and further purified by isocratic FPLC using 0.1 M potassium phosphate buffer pH 7.

**2-Azidoethanamine synthesis.** In a 50 mL round bottom flask, NaN<sub>3</sub> (6.595 g, 101.4 mmol) was dissolved in 30 mL of water and 2-bromoethanamine hydrobromide (7.04 g, 34.3 mmol) was added to the reaction mixture. It was stirred O/N at 80 °C and cooled to 0 °C in an ice bath. To this, 30 mL of diethyl ether was added with 9.00 g (160 mmol) of solid KOH and stirred until the KOH dissolved. The solution was washed 3 $\times$  with ether, the organic phase dried with MgSO<sub>4</sub>, filtered, and the solvent evaporated under reduced pressure. The product was recovered as a yellow oil (95% yield). <sup>1</sup>H NMR (CDCl<sub>3</sub>, 600 MHz)  $\delta$  (ppm): 3.35 (t, 2H, *J* = 5.5 Hz), 2.87 (t, 2H, *J* = 6 Hz).

**FITC-N<sub>3</sub> synthesis.** FITC-N<sub>3</sub> was synthesized as reported in the literature.<sup>40</sup> In a 250 mL flat bottomed flask, 1.53 g (3.93 mmol) of FITC was dissolved in 150 mL of MeOH. 2-Azidoethanamine (0.728 g, 8.45 mmol) was added with

5 mL of TEA. The reaction was stirred at RT O/N and the solvent evaporated the next day and recovered as a dark orange solid (52% yield).  $^1\text{H-NMR}$  ( $\text{CD}_3\text{OD}$ , 500 MHz): 7.99 (d,  $J = 1.95$ , 1H), 7.73 (dd,  $J = 8.15$ ,  $J = 2.05$ , 1H), 7.21 (d,  $J = 8.15$ , 1H), 7.08 (d,  $J = 9.05$ , 2H), 6.65 (d,  $J = 2.20$ , 2H), 6.62 (dd,  $J = 9.08$ ,  $J = 2.23$ , 2H), 3.84 (t,  $J = 5.90$ , 2H), 3.60 (t,  $J = 5.95$ , 2H).

**Synthesis of DB-alkyne (DB-Alk).** Methyl 3,4-dibromo-2,5-dioxo-2,5-dihydro-1H-pyrrole-1-carboxylate was synthesized from a published procedure.<sup>41</sup> 3,4-Dibromomaleimide (1.0 g, 3.9 mmol) and *N*-methylmorpholine (0.43 mL, 3.9 mmol) were dissolved in 35 mL of THF, followed by addition of methylchloroformate (0.30 mL, 3.9 mmol). The reaction was stirred at room temperature (RT) for 20 min. After stirring, 40 mL of DCM was added and the organic phase was washed with water, dried over anhydrous  $\text{MgSO}_4$ , filtered, and solvent was evaporated under reduced pressure to yield a pink solid. Yield: (1.140 g, 94%).  $^1\text{H NMR}$  (500 MHz,  $\text{CDCl}_3$ )  $\delta$  ppm 4.01 (s, 3 H).

Second, to a solution of the previous product, (0.1000 g, 0.3196 mmol) in 4 mL of DCM, propargylamine (0.0250 mL, 0.381 mmol) was added. The reaction was stirred for 20 min, diluted with 10 mL of EtOAc and washed with sat.  $\text{NH}_4\text{Cl}$  ( $\times 2$ ) and water ( $\times 2$ ). The organic phase was dried over anhydrous  $\text{MgSO}_4$ , filtered, and solvent was evaporated under reduced pressure.  $^1\text{H NMR}$  (500 MHz,  $\text{CDCl}_3$ )  $\delta$  (ppm) 2.21 (t,  $J = 2.50$  Hz, 1 H) 4.21 (d,  $J = 2.50$  Hz, 2 H).

**Conjugation of DB-alkyne onto Q $\beta$  (Q $\beta$ -DB-Alk).** Using a 5 mg  $\text{mL}^{-1}$  stock of purified nQ $\beta$ , 200  $\mu\text{L}$  (70.8  $\mu\text{mol}$ ) of the stock was added to 20  $\mu\text{L}$  of a TCEP HCl solution (1.27 M) and incubated for 1 h at RT. To the solution of reduced VLP, 1.74 mL of 0.1 M NaP buffer (pH 5) along with 10  $\mu\text{L}$  of DB-alkyne in DMF (0.6372 M) was added to yield a final concentration of Q $\beta$ : 0.5 mg  $\text{mL}^{-1}$ . The resulting yellow fluorescent solution was washed ( $3\times$ ) in a 10 K MWCO centrifugal spin column with 0.1 M NaP buffer (pH 5) and finally exchanged to 0.1 M KP buffer (pH 7).

**Clicking FITC- $\text{N}_3$  onto DB-alkyne (Q $\beta$ -FITC).** The following 1 mL solutions were prepared;  $\text{CuSO}_4 \cdot 5\text{H}_2\text{O}$  (5 mg, 4 mM), THPTA (22 mg, 41.5 mM), sodium ascorbate (2 mg, 13.3 mM) and aminoguanidine HCl (11 mg, 99.5 mM) in water. For a final Q $\beta$  concentration of 0.5 mg  $\text{mL}^{-1}$  in 0.1 M KP, 10  $\mu\text{L}$  of FITC- $\text{N}_3$  in DMF (16.2 mM) was added to 1 mL of 1 mg  $\text{mL}^{-1}$  Q $\beta$ -DB alkyne. 15  $\mu\text{L}$  of  $\text{CuSO}_4 \cdot 5\text{H}_2\text{O}$  was premixed with 30  $\mu\text{L}$  THPTA and added to the reaction mixture. Finally, 150  $\mu\text{L}$  of aminoguanidine HCl was added followed by 150  $\mu\text{L}$  of sodium ascorbate. The solution was stirred for 3 h on the rotisserie. The resulting green fluorescent solution was washed ( $3\times$ ) in a 10 K MWCO centrifugal spin column with 0.1 M KP buffer (pH 7).

**Synthesis imidazole-1-sulfonyl azide** was synthesized as reported in the literature.<sup>42</sup> Sodium azide (10.1 g, 156 mmol) was placed in a 250 mL round-bottomed flask with a stir bar. The flask was evacuated, a  $\text{N}_2$  atmosphere was introduced, dry acetonitrile (78 mL) was added, and the suspension was cooled to 0  $^\circ\text{C}$ . While the inert atmosphere was maintained, sulfonyl chloride (12.6 mL, 156 mmol) was then added dropwise over the course of at least 10 min with stirring, and the

mixture was slowly warmed to room temperature and stirred for at least 17 h. The suspension was then cooled to 0  $^\circ\text{C}$ , and while the inert atmosphere was maintained, imidazole (20.2 g, 296 mmol) was added continuously over 10 min. The solution was stirred for at least 3 h at 0  $^\circ\text{C}$ , diluted with EtOAc (156 mL), and basified by addition of saturated aqueous  $\text{NaHCO}_3$  (250 mL). The organic layer was then washed with water (250 mL), dried over  $\text{MgSO}_4$ , and filtered. This solution was then cooled to 0  $^\circ\text{C}$  and placed under a  $\text{N}_2$  atmosphere, and concentrated  $\text{H}_2\text{SO}_4$  (3 mL, 156 mmol) was added dropwise over the course of 5 min. The mixture was gradually allowed to warm to room temperature, stirring vigorously. After 24 h, a colorless precipitate had formed. Vacuum filtration followed by a wash with a small amount of cooled EtOAc afforded white crystals which were left to dry for 15 min, then collected in a round-bottom flask, and dried under high vacuum to afford pure product (25.2 g, 93.1 mmol, 60%). The reagent was collected and stored under  $\text{N}_2$  in the fridge.  $^1\text{H NMR}$  ( $\text{DMSO}-d_6$ , 600 MHz)  $\delta$  14.29 (s, br,  $\text{NH}^+$ ), 13.11 (s,  $\text{HSO}_4^-$ ), 9.08 (s, CH), 8.08 (t,  $J = 1.7$  Hz, CH), 7.52 (dd,  $J = 1.7$ , 0.8 Hz, CH).

**Diazo transfer reaction on Q $\beta$ 's free amines (nQ $\beta$ - $\text{N}_3$  or Q $\beta$ -F- $\text{N}_3$ ).** The following solutions were prepared: 14.5 mM  $\text{K}_2\text{CO}_3$ , 4.00 mM  $\text{CuSO}_4 \cdot 5\text{H}_2\text{O}$ , and 7.37 mM imidazole-1-sulfonyl azide salt in water. To 3 mg of unfunctionalized Q $\beta$  (1 mL), 1.68 mL of 0.1 M KP buffer (pH 7) was added followed by 160  $\mu\text{L}$   $\text{K}_2\text{CO}_3$ , 100  $\mu\text{L}$   $\text{CuSO}_4 \cdot 5\text{H}_2\text{O}$ , and 60  $\mu\text{L}$  diazo transfer reagent for a final Q $\beta$  concentration of 1 mg  $\text{mL}^{-1}$ . The solution was stirred overnight at RT and washed ( $5\times$ ) in a 10 K MWCO centrifugal spin column with 0.1 M KP buffer (pH 7). The same was repeated with Q $\beta$ -FITC to yield Q $\beta$ -F- $\text{N}_3$ .

**Synthesis of rhodamine B alkyne.** To a 100 mL round bottom flask, Rhodamine B (2.01 g, 4.28 mmol) was added to 50 mL of DCM. Propargyl alcohol (0.31 g, 5.5 mmol), dicyclohexylcarbodiimide (1.34 g, 6.49 mmol) and 4-dimethylaminopyridine (0.06 g, 500  $\mu\text{mol}$ ) were added and stirred at RT for at least 24 h. Product was purified by column using a gradient of 80:10:10 DCM/acetic acid/methanol (1.35 g, 2.92 mmol, 60%).  $^1\text{H NMR}$  (500 MHz,  $\text{CDCl}_3$ )  $\delta$  (ppm): 1.22 (q, 12H,  $\text{CH}_3$ ), 2.44 (s, 1H,  $\text{CH}=\text{C}$ ), 3.66 (m, 8H,  $\text{CH}_2\text{N}$ ), 4.64 (s, 2H,  $\text{OCH}_2\text{C}=\text{CH}$ ), 6.98–8.24 (m, 10 H).

**Clicking rhodamine-alkyne to Q $\beta$  (Q $\beta$ -RhoB or Q $\beta$ -DBC).** The following 1 mL solutions were prepared;  $\text{CuSO}_4 \cdot 5\text{H}_2\text{O}$  (5 mg, 4 mM), THPTA (22 mg, 41.5 mM), sodium ascorbate (2 mg, 13.3 mM) and aminoguanidine HCl (11 mg, 99.5 mM) in water. For a final Q $\beta$  concentration of 0.5 mg  $\text{mL}^{-1}$  in 0.1 M KP, 10  $\mu\text{L}$  of Rhodamine B - alkyne in DMF (16.2 mM) was added to 1 mL of 1 mg  $\text{mL}^{-1}$  Q $\beta$ - $\text{N}_3$ . 15  $\mu\text{L}$  of  $\text{CuSO}_4 \cdot 5\text{H}_2\text{O}$  was premixed with 30  $\mu\text{L}$  THPTA and added to the reaction mixture. Finally, 150  $\mu\text{L}$  of aminoguanidine HCl was added followed by 150  $\mu\text{L}$  of sodium ascorbate. The solution was stirred for 3 h on the rotisserie. The resulting solution was washed ( $3\times$ ) in a 10 K MWCO centrifugal spin column with 0.1 M KP buffer (pH 7). The resulting fluorescent solution was dialyzed for 3 d in 0.1 M KP buffer (pH 7) at 4  $^\circ\text{C}$ ; buffer refreshed every

6 h. The reaction was repeated using Q $\beta$ -F-N<sub>3</sub> to yield the final product Q $\beta$ -DBC.

**Artificial lysosomal fluid (ALF).** Briefly, sodium chloride (3.210 g), sodium hydroxide (6.000 g), citric acid (20.800 g), calcium chloride (0.097 g), sodium phosphate heptahydrate (0.179 g), sodium sulfate (0.039 g), magnesium chloride hexahydrate (0.106 g), glycerin (0.059 g), sodium citrate dihydrate (0.077 g), sodium tartrate dihydrate (0.090 g), sodium lactate (0.085 g), sodium pyruvate (0.086 g), formaldehyde (1.000 mL, added fresh before use) were dissolved in 200 mL of MilliQ water in order to obtain a 5 $\times$  stock solution. Before use, the solution was diluted to a 1 $\times$  working solution for experimentation.

**Cell uptake and degradation experiments.** MCF-7 cells and RAW 264.7 macrophages cultured in Dulbecco's Modified Eagle Medium (DMEM) supplemented with 10% fetal bovine serum and 1% penicillin/streptomycin were seeded onto glass bottomed dishes (~105 cells per dish). Seeding was performed 1 d before the experiment. The cells were incubated with 10  $\mu$ M solution of the Q $\beta$ -DBC product for 4 h in triplicate. The cells were then washed (3 $\times$ ) with 1 $\times$  PBS, stained with 300 nM Hoescht 33442 dye, washed again (3 $\times$ ) with PBS and 1 mL of clean supplemented media for live cell imaging using an Olympus FV3000 RS Confocal microscope. LysoTracker Deep Red was added to cells when necessary at a concentration of 50 nM, 1 hour prior to cell imaging and washed as previously described.

**Flow cytometry experiments.** MCF-7 cells and RAW 264.7 macrophages cultured in Dulbecco's Modified Eagle Medium (DMEM) supplemented with 10% fetal bovine serum and 1% penicillin/streptomycin were seeded at a concentration of ~106 cells per well in a six well plate. The cells were incubated with 10  $\mu$ M solution of the Q $\beta$ -DBC product for 4 h and were then washed (3 $\times$ ) with 1 $\times$  PBS and clean media was added to the cells. At the appropriate time points, cells were removed from the plates by pipetting and analyzed on a BD Fortessa Flow analyzer.

## Results and discussion

In this work, Q $\beta$  was exploited as a rigid scaffold to create a FRET-based degradation probe through the subsequent functionalization of its cysteine and solvent accessible amine residues. Each of the 180 disulfide bonds that line the pores of the VLP were reduced in the presence of tris 2-carboxyethylphosphine to yield free thiol groups to allow for instant dibromomaleimide re-bridging and the installation of an alkyne functional handle (DBA) without disruption of capsid stability. It has been established that dithiol-maleimide moieties remain susceptible to ligand exchange *via* reverse Michael addition in the presence of thiol rich species such as bovine serum albumin (BSA) and excess glutathione (GSH).<sup>43</sup> This lability can be inhibited by hydrolyzing the maleimide ring to the maleamic acid at a pH  $\geq$  8. Following a three-hour incubation in phosphate buffer at pH 8.5,<sup>44</sup> we tested Q $\beta$ -DBA for

ligand exchange by incubating equivalent amount of VLP and BSA for 24 h and monitoring *via* fast protein liquid chromatography (FPLC) to determine if there was any ligand transfer. Typically, the thiol-maleamic acid group absorbs light at 400 nm and monitoring this in conjunction with monitoring the protein at 280 nm revealed no transfer between Q $\beta$ -DBA and BSA (Fig. S2 $\dagger$ ). With the alkyne handle installed and secure, we employed copper catalyzed azide-alkyne cycloaddition (CuAAC) to attach the first fluorophore—azide functionalized FITC (FITC-N<sub>3</sub>). The dye is introduced to Q $\beta$ -DBA in the presence of copper sulfate, THPTA, aminoguanidine HCl and sodium ascorbate in 0.1 M potassium phosphate buffer to facilitate the click reaction. The resulting solution is easily purified by centrifugal filter to yield a green fluorescent solution of VLPs with approximately 143 fluorophores attached (Fig. 1C top). In order to orthogonally attach the second fluorophore, RhoB, *via* the same CuAAC chemistry, the amine residues were first converted to azide groups. This is achieved by a diazo transfer reaction using water soluble imidazole-1-sulfonyl azide sulfate at room temperature for 16 h. After washing, alkyne functionalized RhoB was attached to the same capsid as FITC-N<sub>3</sub> to yield an orange solution with the attachment of approximately 105 RhoB moieties (Fig. 1C bottom). The final product (Q $\beta$ -DBC) is washed well and dialyzed for several days in an attempt to remove free rhodamine that may be electrostatically bound to the surface of the capsid and characterized. Transmission electron microscopy (TEM) images indicated clearly that the multistep reactions did not alter the icosahedral shape and size of the VLP (Fig. S3 $\dagger$ ). This was further confirmed by dynamic light scattering measurements, in which we found an average particle size of 30  $\pm$  2.1 nm (Fig. S4 $\dagger$ ). We then examined the excitation and emission spectra of FITC and RhoB after attachment to the surface of Q $\beta$ —spectral overlap was observed between the fluorophores (Fig. 1B) confirming appropriate spatial orientation of the fluorophores within the reported Förster distance. To further verify the identity, intactness, and fluorophore activity, non-reducing SDS-PAGE and native agarose gel electrophoresis were performed and analyzed *via* a gel multispectral fluorescence imaging system (Fig. 1D, S5 and 6 $\dagger$ ). The attachment of FITC-N<sub>3</sub> yields green fluorescence (Fig. 1C FITC) which is retained in subsequent reactions (Q $\beta$ -F-N<sub>3</sub> and Q $\beta$ -DBC) The same is observed following the conjugation of RhoB to yield Q $\beta$ -RhoB and the final product—the “double clicked” system—Q $\beta$ -DBC (Fig. 1C). From these data we conclude that the surface of Q $\beta$  was labeled with FRET pairs.

To evaluate the viability of our proposed construct as a sensor for degradation lifetimes in cellular systems, we first subject Q $\beta$ -DBC to 0.1 M potassium phosphate solutions ranging in pH from 3.0–7.4. We found no significant change ( $p \gg 0.5$ ) in the emission intensities of the individual fluorophores or the resulting FRET signal over this pH range, indicating that loss in fluorescence is most likely attributable to the collapse of the particle and not the pH (Fig. 2A). To investigate how FRET would be affected following proteolysis, the sample was incubated with trypsin, a proteolytic enzyme that

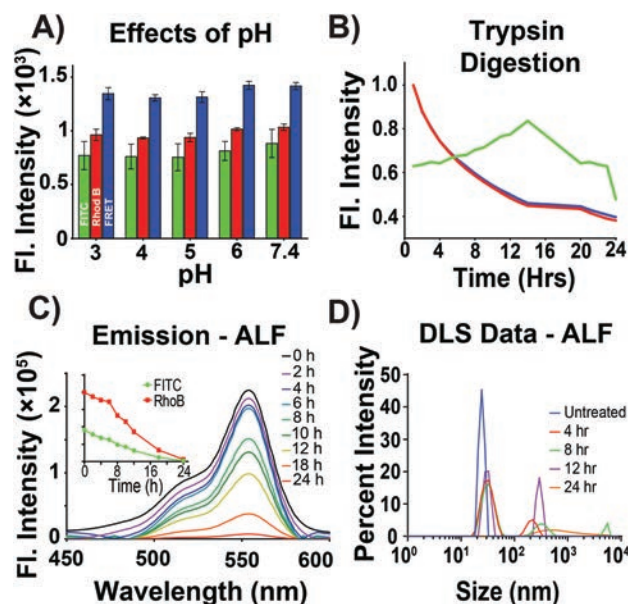


**Fig. 2** All fluorescence data were collected using the following wavelengths and colors: FITC—green ( $\lambda_{\text{ex}}$ : 490 nm/ $\lambda_{\text{em}}$ : 515 nm), Rhodamine—red ( $\lambda_{\text{ex}}$ : 520 nm/ $\lambda_{\text{em}}$ : 560 nm) and FRET—blue ( $\lambda_{\text{ex}}$ : 488 nm/ $\lambda_{\text{em}}$ : 560 nm). (A) Fluorescence intensity at  $\lambda_{\text{max}}$  following incubation of Q $\beta$ -DBC at various pHs in 0.1 M potassium phosphate for 24 h. The data show a statistically insignificant change in emission intensities ( $p \gg 0.5$ ). (B) Q $\beta$ -DBC was incubated with 0.05 M trypsin over the course of 24 h, which produced an initial increase in FITC emission and a concomitant decrease in FRET emission as the FRET pair is separated. Notably, there is decrease in all emission intensities at  $\sim 13$  h, which we attribute to aggregation. (C) FRET emission of the Q $\beta$ -DBC complex in artificial lysosomal fluid (ALF) showing a decrease in total emission. Inset: Decrease in fluorescence emission at  $\lambda_{\text{max}}$  of FITC and RhoB over 24 h. The y-axis is the same as the parent spectra. Select timepoints from this experiment were analyzed by (D) DLS, which shows aggregation of the particle in ALF, most likely attributable to the high ionic strength of the media.

cleaves at the carboxyl side of lysine or arginine residues. Over the course of 24 h, the results depicted in Fig. 2B show an increase in FITC emission (green line) and a decrease in FRET emission (blue line) indicative of an increase of Förster distance. After approximately 14 h there is a sudden decrease in all emission intensities. Analysis of the solution at this time point by DLS found particle precipitation and aggregation. We thus attribute this sudden loss in fluorescence to an aggregation-based quenching of the dyes (Fig. S7 $\dagger$ ).

To further investigate the mechanism of particle disruption, we subjected the Q $\beta$ -DBC complex to artificial lysosomal fluid (ALF). This solution not only mimics the pH, but also the ionic strength, complexity, and crowdedness of the lysosomal compartment to more fully replicate native cellular conditions.<sup>45</sup> Emission spectra collected at different time points and presented in Fig. 2C show a decrease in the intensities of emission at all wavelengths at the same rate. Separation of fluorophores, which is occurring in Fig. 2B, would produce a scenario wherein the FRET emission decreases while the donor fluorophore (FITC) increases. Because all wavelengths were decreasing, we again suspected that the high dielectric

constant of the ALF media causes electrostatically induced aggregation of the VLP (Fig. 2D) and thus quenching of the surface-bound fluorophores. DLS analysis of this VLP in ALF over time showed an increase in particle size from a uniform peak at 30 nm to two peaks of 45 nm and larger agglomerates of approximately 300 nm in a period of four hours. These data predict that, once the VLP enters the cell through receptor mediated endocytosis<sup>46</sup> and is trafficked to an endosomal compartment, we expect to see a loss in FRET and an increase in FITC emission due to proteolysis; however, we also expect to see a loss in total fluorescence owing to electrostatically induced aggregation of the particle.

For our *in vitro* study, RAW 264.7 macrophages and MCF-7 were used as models. Macrophages phagocytose foreign bodies, degrade them rapidly, and then perform other immune related signaling and trafficking to indicate they have consumed a foreign substance.<sup>47</sup> MCF-7, one of the most studied models for cancer research, reproduce and metabolize nutrients quickly.<sup>48</sup> These two cell types have distinct purposes to perform cellular uptake and the fates of these particles following uptake in both cells are almost certainly different. To test this, Q $\beta$ -DBC was incubated with cells at a concentration of 1 mg mL<sup>-1</sup> in supplemented DMEM for four hours and washed (3 $\times$ ) carefully with clean media. Cells destined for confocal imaging were stained with Hoescht 34442 before imaging at select time points. Data presented in Fig. 3 depicts the change in fluorescence intensity of the capsid at four and 24 h after the start of incubation. The macrophages clearly show a large amount of Q $\beta$ -DBC uptake within the first four hours (Fig. 3A) with both fluorophores brightly visible under their respective emission filters and a high FRET signal. This fluorescence intensity fades quickly and is very weak at 24 h (Fig. 3B raw data shown in Fig. S8 $\dagger$ ). Conversely, MCF-7 cells do not readily endocytose as many particles into the lysosomal compartment—much of the fluorescence appears to be diffuse at four hours indicating low localization in an internal compartment (Fig. 3C). To determine where the VLPs were localized, cells were incubated with LysoTracker and imaged live at 4 and 8 h. The results indicate that the particles indeed localize in lysosomal compartments which is indicated by an increase in the Pearson's coefficient. RAW macrophages showed an increase from 0.68 to 0.82 and MCF-7 increased from 0.79 to 0.90 (Fig. S9 $\dagger$ ). After 24 h the emission appears punctate and a similar decrease in emission intensity is observed (Fig. 3D). To more accurately quantify the change in FRET over time, flow cytometry was employed to quantify the emission intensities. After plotting the maximum emission values for each sample (Fig. 3E and F), a trend that mirrors our simulated media emerges. Initially, all fluorescence decreases—which we attribute to an initial cellular uptake and aggregation in the endosome. As time progresses, the FITC signal gradually increases and peaks at approximately 6 h in macrophages and 8 h in MCF-7 cells. We attribute this increase in FITC fluorescence with proteolysis of the VLP into smaller subunits, which increases the distance between the FRET pair. This separation is followed by a sudden crash in the emission

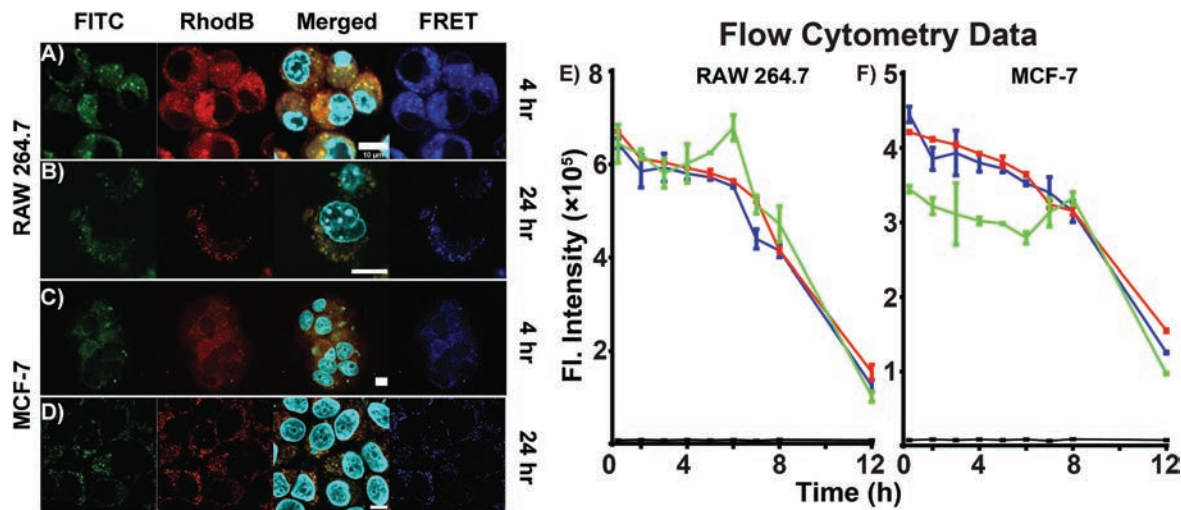


**Fig. 3** Confocal microscopy images processed in NIH ImageJ software of RAW 264.7 macrophages and MCF-7 breast cancer cells at 4 h (A and C) and 24 h (B and D) respectively. There is a visible difference in cellular uptake capacity. Raw image data can be found in Fig. S3.† E and F represent the peak maxes of collected flow cytometry data of RAW 264.7 and MCF-7 cells, showing the same trend in fluorescence trends noted in the previous cell-free degradation assay.

intensities of both fluorophores and the resultant FRET signal. Again, we attribute this to the rapid aggregation of digested fragments. Overall, it appears as though it takes up to 10 h (4 h of incubation, followed by washing, and another 6 h of incubation in clean media) for proteolysis of the VLP to be significant. During that time, however, it appears as though the VLP is aggregating in the endosome/early lysosome. Once proteolysis has begun, it appears as though the resulting protein fragments are quenched relatively shortly thereafter as aggregates.

## Conclusion

Using Q $\beta$  as a scaffold to site-specifically install a FRET pair, we have created a probe for understanding *in vitro* degradation of a virus. We believe our data illustrates that following uptake, VLPs aggregate inside the endosome and that several hours pass before they are degraded by proteolytic enzymes. While our studies do not preclude other dye-specific quenching induced by chemical processes inside the lysosome, the fact that *all* fluorophores quench at the same time leads us to believe that aggregation induced quenching is the culprit. This argument is further made by the fact that the largest loss of fluorescence follows an increase in FITC fluorescence, which we attribute to proteolysis. Further, these cellular results directly reflect our data in simulated cell media, which adds support to our hypothesis that aggregation in the lysosome is happening both before and after proteolysis. Finally, in the tested cell types at least, it appears VLPs have an upper limit of 12 hours before they are effectively destroyed, thus observations beyond this point in these cells would suggest the experimentalist seriously consider these effects as possibly arising from degraded and aggregated VLP products, rather

than intact virions. Possibly decreasing or inhibiting aggregation in the early stages using highly charged amine-rich surfaces may be a method to improve drug or gene delivery from the lysosome.

## Author contributions

ZC and JJG conceptualized the project. CEB, HL and ZC synthesized all compounds. AS performed all NMR spectroscopy. ORB acquired TEM images. ZC acquired fluorescent gel images with the help of SB. CEB collected all remaining data and wrote the manuscript with JJG. DDW supervised SB.

## Conflicts of interest

There are no conflicts to declare.

## Acknowledgements

CEB would like to thank the National Science Foundation Graduate Research Fellows Program (1746053). JJG thanks the National Science Foundation (CAREER DMR-1654405) and the Welch Foundation (AT-1989-20190330) for their generous support. Raw 264.7 macrophages are purchased from ATCC (cat number: ATCC TIB-71) MCF cells were a gift from Dr Jiyong Lee (ATCC HTB-22).

## References

- 1 A. Roldão, M. C. M. Mellado, L. R. Castilho, M. J. T. Carrondo and P. M. Alves, *Expert Rev. Vaccines*, 2010, **9**, 1149–1176.

- 2 T. Vicente, A. Roldão, C. Peixoto, M. J. T. Carrondo and P. M. Alves, *J. Invertebr. Pathol.*, 2011, **107**, S42–S48.
- 3 N. Kushnir, S. J. Streatfield and V. Yusibov, *Vaccine*, 2012, **31**, 58–83.
- 4 Z. Chen, N. Li, S. Li, M. Dharmarwardana, A. Schlimme and J. J. Gassensmith, *Wiley Interdiscip. Rev.: Nanomed. Nanobiotechnol.*, 2016, **8**, 512–534.
- 5 M. Brasino, J. H. Lee and J. N. Cha, *Anal. Biochem.*, 2015, **470**, 7–13.
- 6 J. Guo, X. Zhao, J. Hu, Y. Lin and Q. Wang, *Mol. Pharm.*, 2018, **15**, 2946–2953.
- 7 M. Dharmarwardana, A. F. Martins, Z. Chen, P. M. Palacios, C. M. Nowak, R. P. Welch, S. Li, M. A. Luzuriaga, L. Bleris, B. S. Pierce, A. D. Sherry and J. J. Gassensmith, *Mol. Pharm.*, 2018, **15**, 2973–2983.
- 8 H. Lee, C. E. Benjamin, C. M. Nowak, L. H. Tuong, R. P. Welch, Z. Chen, M. Dharmarwardana, K. W. Murray, L. Bleris, S. D'Arcy and J. J. Gassensmith, *Mol. Pharm.*, 2018, **15**, 2984–2990.
- 9 M. J. Rohovie, M. Nagasawa and J. R. Swartz, *Bioeng. Transl. Med.*, 2017, **2**, 43–57.
- 10 N. Suthiwangcharoen, T. Li, K. Li, P. Thompson, S. You and Q. Wang, *Nano Res.*, 2011, **4**, 483–493.
- 11 A. E. Czapar, Y.-R. Zheng, I. A. Riddell, S. Shukla, S. G. Awuah, S. J. Lippard and N. F. Steinmetz, *ACS Nano*, 2016, **10**, 4119–4126.
- 12 L. Chen, Y. Wu, Y. Lin and Q. Wang, *Chem. Commun.*, 2015, **51**, 10190–10193.
- 13 E. A. Jares-Erijman and T. M. Jovin, *Nat. Biotechnol.*, 2003, **21**, 1387–1395.
- 14 L. Yuan, W. Lin, K. Zheng and S. Zhu, *Acc. Chem. Res.*, 2013, **46**, 1462–1473.
- 15 G. Chen, F. Song, X. Xiong and X. Peng, *Ind. Eng. Chem. Res.*, 2013, **52**, 11228–11245.
- 16 K. V. Rao, K. K. R. Datta, M. Eswaramoorthy and S. J. George, *Chem. – Eur. J.*, 2012, **18**, 2184–2194.
- 17 Y. Gambin and A. A. Deniz, *Mol. Biosyst.*, 2010, **6**, 1540–1547.
- 18 B. Schuler and W. A. Eaton, *Curr. Opin. Struct. Biol.*, 2008, **18**, 16–26.
- 19 A. Kitamura, K. Nagata and M. Kinjo, *Int. J. Mol. Sci.*, 2015, **16**, 6076–6092.
- 20 S. Song, M. J. Hanson, B.-F. Liu, L. T. Chylack and J. J. N. Liang, *Mol. Vision*, 2008, **14**, 1282–1287.
- 21 S. Hoffmann, C. Gorzelanny, B. Moerschbacher and F. M. Goycoolea, *Nanomaterials*, 2018, **8**, 846.
- 22 L. Zhang, N. G. Gurskaya, E. M. Merzlyak, D. B. Staroverov, N. N. Mudrik, O. N. Samarkina, L. M. Vinokurov, S. Lukyanov and K. A. Lukyanov, *BioTechniques*, 2007, **42**, 446–450.
- 23 Y.-J. Lee, S. Datta and J.-P. Pellois, *J. Am. Chem. Soc.*, 2008, **130**, 2398–2399.
- 24 Z. S. Pehlivan, M. Torabfam, H. Kurt, C. Ow-Yang, N. Hildebrandt and M. Yüce, *Microchim. Acta*, 2019, **186**, 563.
- 25 Y. Luo, F. Liu, E. Li, Y. Fang, G. Zhao, X. Dai, J. Li, B. Wang, M. Xu, B. Liao and G. Sun, *Biosens. Bioelectron.*, 2020, **148**, 111832.
- 26 C. E. Benjamin, Z. Chen, P. Kang, B. A. Wilson, N. Li, S. O. Nielsen, Z. Qin and J. J. Gassensmith, *J. Am. Chem. Soc.*, 2018, **140**, 17226–17233.
- 27 M. L. Hovlid, J. L. Lau, K. Breitenkamp, C. J. Higginson, B. Laufer, M. Manchester and M. G. Finn, *ACS Nano*, 2014, **8**, 8003–8014.
- 28 J. K. Pokorski, M. L. Hovlid and M. G. Finn, *ChemBioChem*, 2011, **12**, 2441–2447.
- 29 J. K. Pokorski and N. F. Steinmetz, *Mol. Pharm.*, 2011, **8**, 29–43.
- 30 Z. Chen, N. Li, L. Chen, J. Lee and J. J. Gassensmith, *Small*, 2016, **12**, 4563–4571.
- 31 T. Storni, C. Ruedl, K. Schwarz, R. A. Schwendener, W. A. Renner and M. F. Bachmann, *J. Immunol.*, 2004, **172**, 1777–1785.
- 32 Z. Yin, M. Comellas-Aragones, S. Chowdhury, P. Bentley, K. Kaczanowska, L. Benmohamed, J. C. Gildersleeve, M. G. Finn and X. Huang, *ACS Chem. Biol.*, 2013, **8**, 1253–1262.
- 33 S. M. Goldinger, R. Dummer, P. Baumgaertner, D. Mihic-Probst, K. Schwarz, A. Hammann-Haenni, J. Willers, C. Geldhof, J. O. Prior, T. M. Kundig, O. Michielin, M. F. Bachmann and D. E. Speiser, *Eur. J. Immunol.*, 2012, **42**, 3049–3061.
- 34 T. M. Kundig, L. Klimek, P. Schendzielorz, W. A. Renner, G. Senti and M. F. Bachmann, *Curr. Treat. Options Allergy*, 2015, **2**, 72–82.
- 35 A. Jegerlehner, F. Zabel, A. Langer, K. Dietmeier, G. T. Jennings, P. Saudan and M. F. Bachmann, *PLoS One*, 2013, **8**, e78947.
- 36 R. P. Welch, H. Lee, M. A. Luzuriaga, O. R. Brohlin and J. J. Gassensmith, *Bioconjugate Chem.*, 2018, **29**, 2867–2883.
- 37 Z. Chen, S. D. Boyd, J. S. Calvo, K. W. Murray, G. L. Mejia, C. E. Benjamin, R. P. Welch, D. D. Winkler, G. Meloni, S. D'Arcy and J. J. Gassensmith, *Bioconjugate Chem.*, 2017, **28**, 2277–2283.
- 38 Y. Li, M. S. Budamagunta, J. Luo, W. Xiao, J. C. Voss and K. S. Lam, *ACS Nano*, 2012, **6**, 9485–9495.
- 39 D. A. Hiller, J. M. Fogg, A. M. Martin, J. M. Beechem, N. O. Reich and J. J. Perona, *Biochemistry*, 2003, **42**, 14375–14385.
- 40 C. Gnaccarini, W. Ben-Tahar, A. Mulani, I. Roy, W. D. Lubell, J. N. Pelletier and J. W. Keillor, *Org. Biomol. Chem.*, 2012, **10**, 5258–5265.
- 41 L. Castaneda, Z. V. Wright, C. Marculescu, T. M. Tran, V. Chudasama, A. Maruani, E. A. Hull, J. P. Nunes, R. J. Fitzmaurice, M. E. Smith, L. H. Jones, S. Caddick and J. R. Baker, *Tetrahedron Lett.*, 2013, **54**, 3493–3495.
- 42 G. T. Potter, G. C. Jayson, G. J. Miller and J. M. Gardiner, *J. Org. Chem.*, 2016, **81**, 3443–3446.
- 43 M. E. B. Smith, F. F. Schumacher, C. P. Ryan, L. M. Tedaldi, D. Papaioannou, G. Waksman, S. Caddick and J. R. Baker, *J. Am. Chem. Soc.*, 2010, **132**, 1960–1965.

- 44 Z. Chen, N. Li, L. Chen, J. Lee and J. J. Gassensmith, *Small*, 2016, **12**, 4563–4571.
- 45 A. MilosevicAc, J. Bourquin, D. Burnand, P. Lemal, F. Crippa, C. A. Monnier, L. Rodriguez-Lorenzo, A. Petri-Fink and B. Rothen-Rutishauser, *Chimia*, 2019, **73**, 55–58.
- 46 F. A. Galaway and P. G. Stockley, *Mol. Pharm.*, 2013, **10**, 59–68.
- 47 M. A. Elhelu, *J. Natl. Med. Assoc.*, 1983, **75**, 314–317.
- 48 A. L. Meadows, B. Kong, M. Berdichevsky, S. Roy, R. Rosiva, H. W. Blanch and D. S. Clark, *Biotechnol. Prog.*, 2008, **24**, 334–341.